Sustainable Energy Technologies and Assessments 46 (2021) 101230

Contents lists available at ScienceDirect

Sustainable Energy Technologies and Assessments

journal homepage: www.elsevier.com/locate/seta

Concurrent optimization and 4E analysis of organic Rankine cycle power plant driven by parabolic trough collector for low-solar radiation zone

Oguz Arslan *, Damla Kilic

Mechanical Engineering Department, Engineering Faculty, Bilecik Seyh Edebali University, 11230 Bilecik, Turkey

ARTICLE INFO

Keywords:
Exergy
Low radiation zone
Net present value
Organic rankine cycle
Parabolic trough collector

ABSTRACT

The Organic Rankine Cycle driven by parabolic trough collectors for the low-solar radiation zone was investigated in this study. Six environment-friendly refrigerants namely R152a, R600a, R601a, cyclopentane, cyclohexane, toluene were evaluated. In addition, the conventional Rankine cycle was evaluated. The dynamic energy and exergy analysis based on the daily average solar data was conducted. The system was designed in a combination solar field, thermal energy storage subsystem, and power block for 24 h of working time without any external energy source. The designed system was concurrently optimized through the economic indicator namely net present value since all the parameters depend on each other. The best design was obtained for conventional cycle with a net present value of 9.012 million US$. The optimum pressure and temperature of the turbine inlet were determined as 3250 kPa and 380 oC, respectively. The optimal ratio of the heat transfer fluid was found around 34.1%. The maximum energy and exergy efficiencies were respectively obtained as 11.05% and 11.86%. These values were respectively conducted as 10.19% and 10.94% at the design point. It was also conducted that the reductions in the emissions of CO2, SO2, and NOx were 108,046.4 ktones, 2,457.6 ktones, and 249.7 ktones, respectively.

Introduction

In the last decades, power generation from renewable energy sources became an urgent issue from the view of environmental concerns. The countries started to make their national renewable investment plans considering their potentials for renewable energy sources. From this point of view, not all regions are available since their resources are limited or unavailable. In a large range of the world, solar energy seems it is the best or single alternative renewable source. Thus, it is very important to evaluate the investment plans sensitively for the future planning of locations with low-radiation. One of the most useful ways for the evaluation of solar energy is to use concentrated collectors, which make the collected radiation increase in a particular area. In this aim, the power plant with an Organic Rankine Cycle (*ORC*) driven by parabolic trough collectors (*PTC*) is one of the alternative solutions for the low-radiation zones. However, for a respectable investigation, the systems should be carefully investigated from the energy, economics, and environmental points of view [1–3].

ORC is commonly used in power generation systems using different energy sources and working fluids. Zhang et al. [4] investigated the *ORC* power plant driven by the waste heat at 250 °C. They used cyclohexane as the working fluid. In the study, the energy and exergy efficiencies were reported as 22% and 60%, respectively. Wand et al. [5] used R245fa as the working fluid and reported an energy efficiency of 9.5% for the heat source of waste heat with 133.5 °C. Ozahi et al. [6] used toluene as the working fluid and reported an exergy efficiency of 15.69% for the heat source of waste heat with 566 °C. Gao et al. [7] used R123 as the working fluid and reported an energy efficiency of 17.85% for the heat source of waste heat with 130 °C. Abrosimov et al. [8] used R601 as the working fluid and reported an energy efficiency of 9.84% for the heat source of waste heat with 520 °C.

Arslan et al. [9] investigated *ORC* power plant driven by geothermal energy. They used R141b as the working fluid for a heat source at 133.5 °C. In the study, the energy efficiency was reported as 16.31%. Moloney et al. [10] used R1233zd(E) as the working fluid and reported respectively an energy and exergy efficiency of 16.2% and 52.3% for the heat source of geothermal energy with 251 °C. Mokarram and Mosaffa [11] used R245fa as the working fluid and reported respectively an energy and exergy efficiency of 14.66% and 55.15% for the heat source of geothermal energy with 250 °C. Yadav and Sircar [12] used R134a as the working fluid and reported an energy efficiency of 8.0% for the heat

* Corresponding author.
E-mail address: oguz.arslan@bilecik.edu.tr (O. Arslan).

https://doi.org/10.1016/j.seta.2021.101230
Received 24 January 2021; Received in revised form 8 March 2021; Accepted 1 April 2021
Available online 21 April 2021

Nomenclature

A	Area (m^2)
B_t	Cash flow ($)
C	Cost ($)
c_p	Specific heat capacity (kJ/kgK)
D	Diameter (m)
$\dot{E}$	Energy (kW)
$\dot{E}x$	Exergy (kW)
F_R	Heat removal factor
F'	Collector efficiency factor
H	Height (m)
h	Enthalpy (kJ/kg)
I_b	Beam solar radiation (W/m^2)
L	Length (m)
m	Mass of the oil in the tank (kg)
$\dot{m}$	Mass rate (kg/s)
N	Number of collectors
P	Pressure (kPa)
$\dot{Q}$	Heat energy (kW)
r	Discount rate
S	Heat absorbed by the receiver (kWh)
s	Entropy (kJ/kg)
T	Temperature (^oC, K)
U	Overall heat coefficient (W/m^2K)
U_L	Heat loss coefficient (W/m^2K)
$\dot{W}$	Power (kW)
x	Mass ratio (%)

Greek Symbols

α_r	Absorptivity of receiver
ε	Exergy efficiency(%)
γ	Intercept factor
γ_{HL}	Tank loss coefficient (W/m^2K)
η	Energy efficiency(%)
θ	Incidence angle
κ	Incidence angle modifier
τ_{cover}	Transmissivity of the cover glazing
τ_{PTC}	Effective transmissivity of thePTC
ψ	Specific exergy(kJ/kg)

Subscripts

0	Reference state
a	Aperture
amb	Ambient
d	Destruction
elec	Electricity
i	Input, Initial investment, inner
mr	Maintenance and repair
ms	Molten salt
o	Output, outer
p	Pump, Personnel expenses
r	Receiver
t	Total, Tank
u	Useful
wf	Working fluid

Abbreviations

C	Condenser
CRC	Conventional Steam Rankine Cycle
CST	Cold Storage Tank
DNI	Direct Normal Irradiance
GWP	Global Warming Potential
HE	Heat Exchanger
HST	Hot Storage Tank
NPV	Net Present Value
ODP	Ozone Depletion Potential
ORC	Organic Rankine Cycle
PB	Power Block
PTC	Parabolic Trough Collector
SF	Solar Field
T	Turbine
TES	Thermal Energy Storage

source of geothermal energy with 85 °C. Noroozian et al. [13] used CO_2 as the working fluid and reported respectively an exergy efficiency of 46.13% for the heat source of geothermal with low temperature. Wang et al. [14] used the zeotropic mixture (R600a-R601) as the working fluid and reported respectively an energy and exergy efficiency of 11.24% and 49.37% for the heat source of geothermal energy with 168 °C.

Yang et al. [15] investigated *ORC* power plant driven by solar energy. They used toluene as the working fluid for a heat source at 400 °C. In the study, the energy efficiency was reported as 17.9%. Roumpedakis et al. [16] used R152a as the working fluid for the solar heat source at 570 °C. In the study, the maximum exergy efficiency was reported as 6.0%. Wang et al. [17] used R123 as the working fluid and reported an energy efficiency of 7.79% for the heat source of solar with 90 °C. Abdollahpour et al. [18] used CO_2 as the working fluid and reported an exergy efficiency of 8.53% for the heat source of solar with 187 °C. Habka and Ajib [19] used a mixture namely R401B as the working fluid and reported an energy efficiency of 5.30% for the heat source of solar with 90 °C.

In the proposed systems, the temperature of the heat source (T_{source}) ranges from 70 °C to 570 °C. Depending on the temperature of heat sources, many working fluids were performed including all the types of wet, dry, or isentropic fluids. For the high-temperature applications ($T_{source} > 300$ °C), the most appropriate fluids were conducted as toluene [20], cyclopentane [21], and m-xylene [22]. For the medium temperature ($150 < T_{source} < 300$ °C) applications, the most appropriate fluids were conducted as cyclohexane [4], R1233zd(E) [10], R245fa [23], R601a [24], and Heptane [25]. For the low temperature ($T_{source} <$ 150 °C) applications, the most appropriate fluids were conducted as R123 [17], R152a [24], R141b [26], R134a [27], and R600a [28]. The different collector technologies such as flat plate collector [17], compound parabolic involute collector [29], Fresnel reflector technology [30], Dish concentrator [31], and parabolic trough collector [32] were also conducted for *ORC* applications.

In the literature, thermodynamic and economic analyses of *ORC* were conducted for a certain solar radiation value of medium to high ranging from 400 W/m^2 to 1000 W/m^2. The formed designs were also commonly based on thermal energy storage (*TES*) including limited working hours. The designs on the full daily time (24 h) were built on the usage of an external energy source such as oil for higher solar irradiation values. The availability of *ORC* based on solar energy without an external source and operating under the low solar irradiation (<400 W/m^2) is still intriguing. In this study, an *ORC* power plant powered by low solar irradiation is analyzed and optimized. Bilecik province (DNI ranging from 241 to 398 W/m^2) is the selected pilot area for the installation of the plant. The working conditions are set for a working time of 24 h without any external energy source. The system is formed of three subsystems namely solar field (*SF*) driven by *PTC*, *TES,* and *ORC* power block (*PB*). Then, the system is analyzed from the energy, exergy,

environmental, and economics (4E) points of view. The net present value (*NPV*) method is used for a lifetime of 20 years in economic evaluation since it gives a possibility to evaluate the time value of the money. Finally, the results of *NPV* are used as the objective function for the concurrent optimization of the system operating with the different working fluids.

Study area

Bilecik province was selected as the study area. Bilecik, with a population of 223,446 and a surface area of 4,307 km^2, is located at 40.1° latitude and 29.9° longitude. Bilecik has a low solar radiation value ranging between 1400 and 1550 kWh/m^2 per year (DNI of 241 to 398 W/m^2) with an insolation time ranging between 2.98 and 10.68 has seen in Fig. 1 [33,34].

From the viewpoint of geographical conditions, Bilecik has a mountainous and rugged terrain. Therefore, there are limited options to install a power plant in the area. The available installation field was determined taking factors such as distance to the electricity transmission line, shading issues, preventing cultivated and woodland areas into account. The satellite image of the determined field is given in Fig. 2.

The determined study area has a perimeter of 9.616.69 m and a surface area of 2.77 km^2 which a part of 2.5 km^2 is used for *SF*. Bilecik has an average (calculated on daily basis using the data of the last 10 years) ambient temperature (T_{amb}) ranging between −2.4 and 25.6 °C. The maximum temperature was recorded as 41 °C in the period of the last 80 years [31]. The solar data is given in Fig. 3 [33–35].

The beam solar radiation (I_b) ranges between 0.94 and 2.91 kWh/m^2-day. While the lowest value was recorded in December, the highest value was observed in June. Insolation time changes between 2.98 and 10.63 h. The highest insolation time is recorded in July where the yearly solar irradiation is about 1469 kWh/m^2-year for a clearness factor of 0.33.

System description

ORC plant driven *by PTC* is formed of three subsystems namely solar

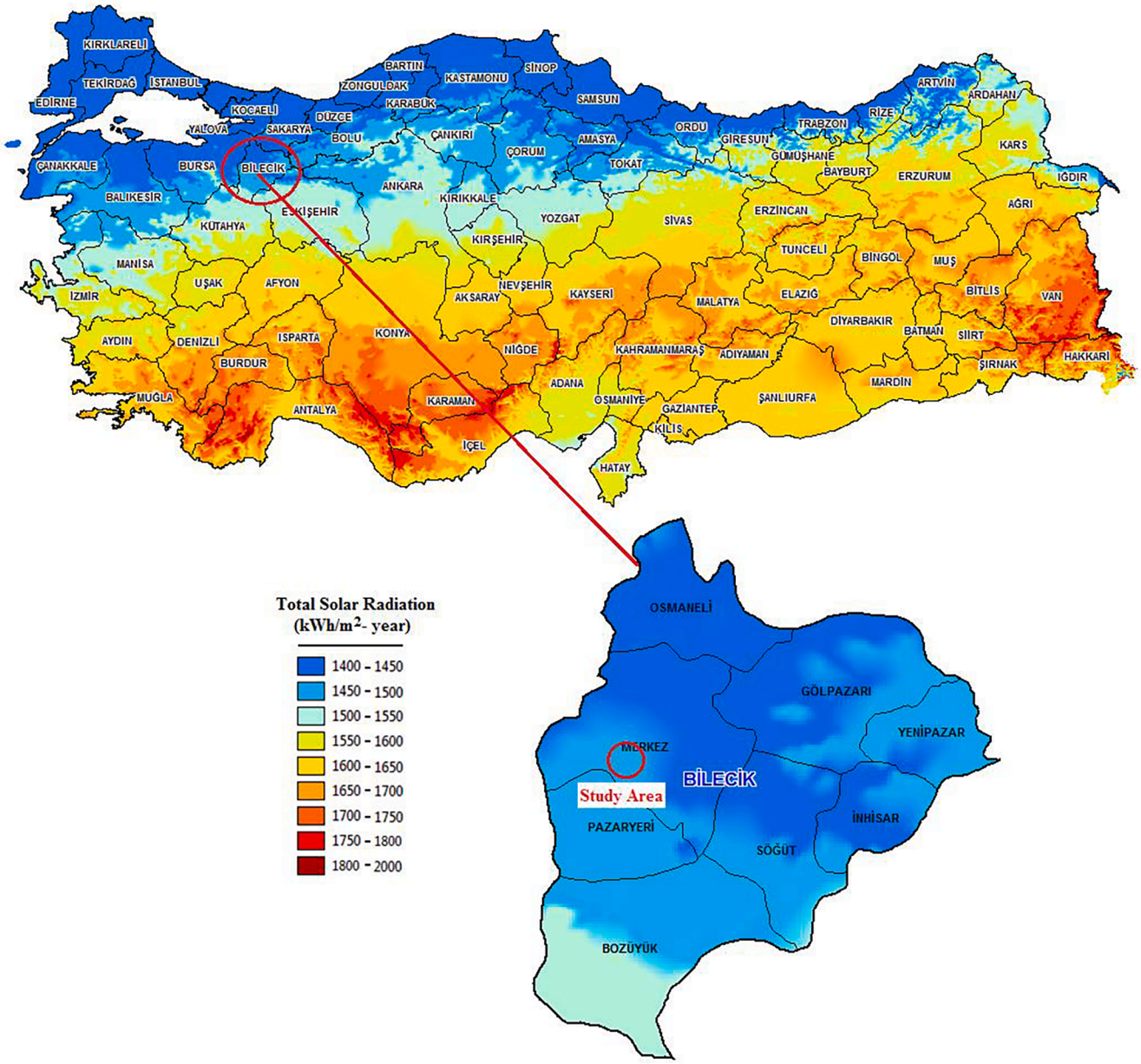

Fig. 1. Solar atlas of Turkey and Bilecik [33,34].

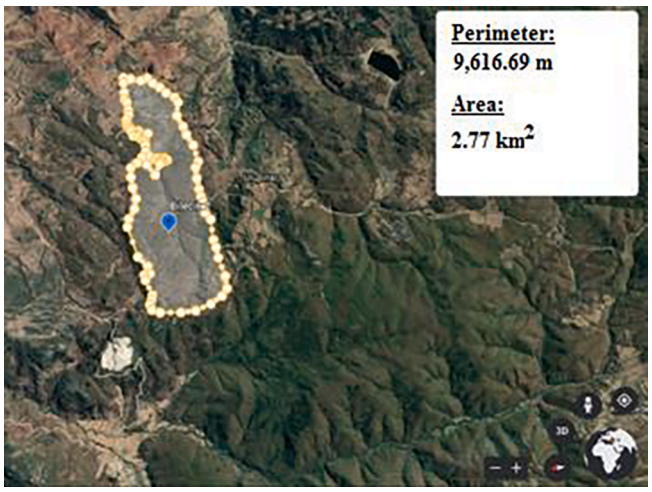

Fig. 2. The study area of the power plant.

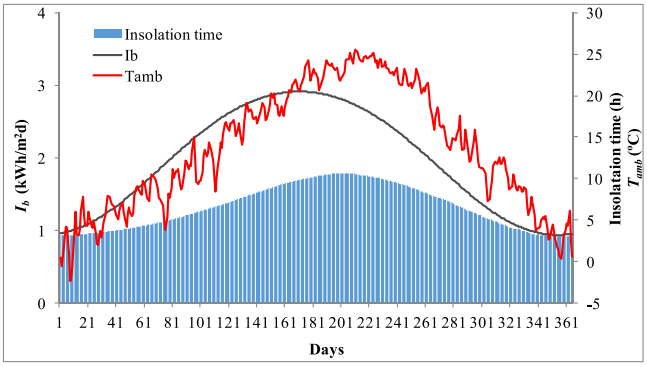

Fig. 3. Daily average data for Bilecik [33–35].

field (*SF*), thermal energy storage (*TES*), and power block (*PB*). The flow diagram is given in Fig. 4.

The solar rays focus on the receiving pipe in the center of *PTC*, which are later converted to heat energy. In insolation time, some of this heat energy (in a mass ratio of 1-*x*) is transferred to *TES* subsystem by a heat exchanger (HE-I) while the remaining part (in a mass ratio of *x*) is transferred to *PB* subsystem to generate electricity generation by another heat exchanger (HE-III). For the out of insolation time, the *PB* is fed from *TES*. At this stage, the stored energy is transferred to *PB* by the heat exchanger of HE-I. The working time is set for 24 h considering the design point. So, the variable mass ratios of *TES* and working fluid are regulated by the frequency-controlled pumps according to the characteristic points obtained for the optimal design. All the pump efficiencies are included as 80% into calculations. Considering the worst climatic conditions in Bilecik province, the efficiency of heat exchangers is introduced as 98% into calculations. By doing so, a heat loss of 2% in heat sink fluid is taken into account.

Solar field (SF)

In *SF*, parabolic trough type collector (*PTC*) is selected in accordance with studied parametric conditions. *PTC* can be oriented in the east to west (E-W) direction tracking the sun from north to south (N-S) or in N-S direction tracking the sun in E-W. Over a single-year period, a horizontal N-S trough field usually collects slightly more energy than a horizontal E-W one [36]. Therefore, it is assumed that the collectors are located in the N-S direction with a solar tracking system in the direction of E-W. Taking the shading effect into account, a distance of about 5.1 m between the *PTC* lines was adapted into calculations to determine the collector numbers [37]. The collector number is determined as 15489.

Table 1
Technical properties of *PTC* [32,38].

Parabolic Collectors	Values
Receiver outer diameter ($D_{o,r}$)	0.07 m
Receiver inner diameter ($D_{i,r}$)	0.066 m
Glass envelope outer diameter ($D_{o,g}$)	0.120 m
Glass envelope inner diameter ($D_{i,g}$)	0.115 m
Heat transfer coefficient inside the receiver (h_{fi})	300 W/m^{2}K
Thermal conductivity of the receiver (k)	16 W/mK
Transmissivity of the cover glazing (τ_{cover})	0.90
Effective transmissivity of *PTC* (τ_{ptc})	0.94
Absorptivity of receiver (α_r)	0.87
Intercept factor (γ)	0.95
Single collector width (W)	5.76 m
Single collector length (L)	15 m
Concentration Ratio (CR)	47

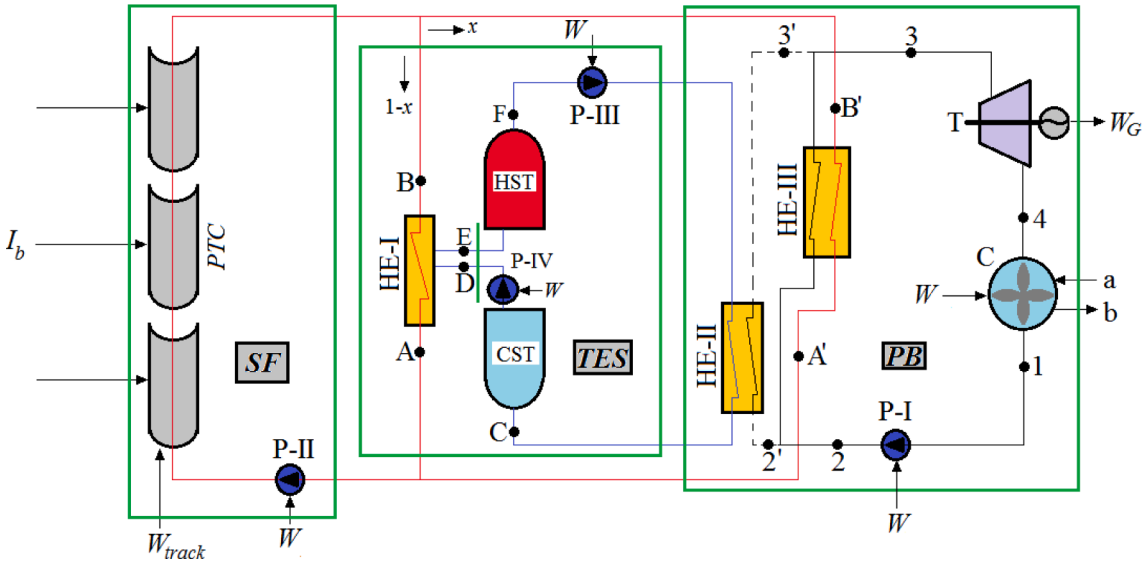

Fig. 4. Flow diagram of the system.

The technical details of the *PTC* used in system design are given in Table 1 [32,38].

Thermal energy storage system (TES)

In the *TES* system, an indirect type is selected compatible with the working principle. Two tanks namely hot storage (*HST*) and cold storage (*CST*) are used in the system. In this regard, it is possible to run the system directly during insolation by the heat potential of heat transfer fluid in the mass ratio of x. At the out of the insolation time, the stored heat in *HST* is used by the discharge process. The discharged fluid from *HST* is charged into *CST* to complete the cycle. Therefore, the sizes of the tanks are determined concerning the maximum yearly requirement that is determined on daily basis values. In Table 2, the technical characteristics of *TES* are given.

ORC power block (PB)

ORC power block includes six main components namely heat exchangers (HE-II and HE-III), turbine (T), generator (G), pump (P-I), and condenser (C). *ORC* is fed by HE-III in insolation time and by HE-II in non-insolation time. Turbine efficiency and pump efficiencies are respectively included as 85% and 80% into calculations. Since there is no source for the cooling water, the dry type (air) cooling is taken into account. In this regard, assuming a minimum temperature difference of 8–10 °C between inlet and outlet points, the outlet temperature of cooling air is set to 35 °C where the inlet conditions change according to the meteorological data given in Fig. 3. Besides, the outlet conditions of the working fluid are determined in accordance with the recorded highest temperature value of 41 °C [35], and a suitable pinch point of 15 °C [39]. Therefore, the condensation temperature of any working fluid is set to 56 °C. Thus, the initial points for the optimization process are obtained considering the extreme conditions.

Selection of working fluids

In the *SF*, a thermic oil named Therminol-VP1 is selected as heat transfer fluid since it is thermally stable and suitable for operation over long periods at bulk temperatures up to 370–400 °C [40]. In *TES*, Molten salt with a low melting point (17.50 wt% $LiNO_3$, 14.18 wt% $NaNO_3$, 50.53 wt% KNO_3, and 17.78 wt% $NaNO_2$) is used as the storage material. It is chosen because of its desired properties such as lower freezing, higher heat capacity, higher upper limit temperature, higher long-term thermal stability (total weight loss of 7.1%), lower corrosion behavior, lower cost, and higher thermal conductivity (0.55 W/mK) [41]. In *PB*, taking the *p-v-T* behavior, thermal stability, and environmental issues of the fluids into consideration, seven different working fluids namely R152a, R-600a, R601a, R718, cyclopentane, cyclohexane, and toluene are selected covering the best of the high, medium, and low-temperature applications. The properties of the fluids used in the handled system are given in Table 3 [40–43].

Thermodynamic evaluation

Neglecting the kinetic energy and potential energy terms, the energy balance of the system for the steady-state conditions is given as:

Table 2
Properties of *HST* and *CST*.

Property	Value
Tank Diameter; D_t (m)	30.0
Tank Height; H (m)	9.2
Tank heat loss coefficient; γ_{HL} (W/m^{2}K)	0.6
Tank volume; V (m^3)	6476.3
Maximum mass, m (tones)	10288.2

$$I_b - \dot{Q}_{SF} - \dot{Q}_{TES} - \dot{Q}_{PB} + \dot{W}_{aux} - \dot{W}_G + \dot{m}_a h_a - \dot{m}_b h_b = 0 \quad (1)$$

where I_b, $\dot{Q}_{SF}$, $\dot{Q}_{TES}$, $\dot{Q}_{PB}$, $\dot{W}_{aux}$ and $\dot{W}_G$ represent the direct normal (beam) irradiation (DNI), heat losses of *SF*, heat losses of *TES*, heat losses of *PB*, power of auxiliary equipment including pumps and condenser blower, and generated power, respectively. The term; h indicates enthalpy of the airflow at the condenser. The exergy balance of the system is then given as:

$$\dot{E}x_{solar} - \dot{E}x_{SF}^{Q} - \dot{E}x_{TES}^{Q} - \dot{E}x_{PB}^{Q} + \dot{E}x_{aux}^{W} - \dot{E}x_{G}^{W} + \dot{m}_a\psi_a - \dot{m}_b\psi_b = \dot{E}x_d \quad (2)$$

where $\dot{E}x_{solar}$, $\dot{E}x_{SF}^{Q}$, $\dot{E}x_{TES}^{Q}$, $\dot{E}x_{PB}^{Q}$, $\dot{E}x_{aux}^{W}$, $\dot{E}x_{G}^{W}$ and $\dot{E}x_d$ represent the exergy rates of solar irradiation, heat losses of *SF*, *TES*, *PB*, the exergy of auxiliary equipment, the exergy of generator, and exergy destruction rate, respectively. The superscript Q and W denote respectively the exergy related to heat and work where ψ describes the specific exergy of the flow respectively. The expressions are given as follows:

$$\dot{E}x^{Q} = \left(1 - \frac{T_0}{T}\right) \cdot \dot{Q} \quad (3)$$

$$\dot{E}x^{W} = \dot{W} \quad (4)$$

$$\psi = (h - h_0) - T(s - s_0) \quad (5)$$

where h is enthalpy as mentioned before and s is the entropy. The subscript "0″ identifies the reference state conditions that are taken as 25 °C and 1 atm for this study. $\dot{E}x_{solar}$ is the exergy of solar radiation and given by [44]:

$$\dot{E}x_{solar} = I \cdot \left[1 + \frac{1}{3}\left(\frac{T_o}{T_{sun}}\right)^4 - \frac{4}{3}\left(\frac{T_o}{T_{sun}}\right)\right] \quad (6)$$

where $T_{sun}$is the temperature of the sun and taken as 5800 K in this study [45]. In this regard, the energy and exergy efficiencies of the system are given as:

$$\eta = \frac{\dot{W}_{net}}{I} \quad (7)$$

$$\varepsilon = \frac{\dot{W}_{net}}{\dot{E}x_{solar}} \quad (8)$$

Thermodynamic analysis of SF

The energy balance of *SF* is given by:

$$I - \dot{Q}_{PTC} - \dot{Q}_{\mathrm{HE-II}} + \dot{W}_{\mathrm{P-II}} + \dot{W}_{track} + \dot{m}_{A'} h_{A'} + \dot{m}_D h_D - \dot{m}_{B'} h_{B'} - \dot{m}_E h_E = 0 \quad (9)$$

In Eq. (9), the term "$I - \dot{Q}_{PTC}$"describes the rate of useful energy ($\dot{Q}_u$) of a single collector, and is given by [46]:

$$\dot{Q}_u = N \cdot F_R \cdot A_r \cdot [S \cdot CR - \pi \cdot U_L \cdot (T_E - T_{amb})] \quad (10)$$

where N is the number of *PTC*, F_R is the heat removal factor, S is the heat absorbed by the receiver. U_L, $T_E$and T_{amb} are the heat loss coefficient, the inlet temperature of heat transfer fluid temperature, and the ambient temperature, respectively. *CR*, which is described as the ratio of aperture area (A_a) to receiver area (A_r), is the concentration ratio of the *PTC*. It is given as follows in terms of the width of the collector (D_r) and glass covering outlet diameter ($D_{o,g}$):

$$CR = \frac{A_a}{A_r} = \frac{(D_r - D_{o,g})}{D_{o,g}} \quad (11)$$

Since the value of *CR* is greater than 10, the diffuse radiation is neglected [46]. So, the heat absorbed by the receiver; S is defined as

Table 3
Properties of fluids used in system design [40–43].

Properties	R152a	R600a	R601a	Cyclopentane	Cyclohexane	R718	Toluene	Therminol VP-1	Molten Salt
p-v-T behavior	Wet	Dry	Dry	Dry	Dry	Wet	Dry	–	–
Boiling Point (°C)	−24.0	−11.7	27.8	49.3	80.7	100.0	110.6	257.0	–
Critical Temperature (°C)	113.3	134.7	187.2	238.5	280.5	374.0	318.6	430	–
Critical Pressure (MPa)	4.52	3.63	3.38	4.52	4.08	22.06	4.13	–	–
Density (kg/m^3)	812.3*	508.7*	582.0*	708.9*	744.0*	985.2	851	1068	1920
Specific heat (kJ/kgK)	2.01*	2.67*	2.45*	1.96*	2.01*	4.18*	1.70	2.70	1.66
Melting temperature (°C)	–	–	–	–	–	–	–	–	99
ODP**	0	0	0	0	0	0	0	–	–
GWP***	124	~20	~20	~20	~20	0	~20	–	–

*values at 56 °C, ** relative to R11, ***relative to CO_2.

[36]:

$$S = I_b \cdot \eta_r \tag{12}$$

where I_b is the beam solar irradiation. η_r is the optical efficiency and given as [36];

$$\eta_r = \tau_{cover} \cdot \alpha_r \cdot \rho_{PTC} \cdot \gamma \cdot \kappa(\theta) \tag{13}$$

Here, τ_{cover} is the transmissivity of the glazing cover of the receiver, α_r is absorptivity of the receiver, ρ_{PTC} is the reflectance of the mirror, γ is the intercept factor. $\kappa(\theta)$ is the incidence angle modifier and given as [36,46]:

$$\kappa(\theta) = 1 - 2.2307x10^{-4} \cdot \theta - 1.1x10^{-4} \cdot \theta^2 + 3.18596x10^{-6} \cdot \theta^3 - 4.85509x10^{-8} \cdot \theta^4 \tag{14}$$

where θ, indicates the incident angle. The angle of incidence for the horizontal N-S axis with E-W tracking calculated as [36]:

$$\cos(\theta) = \sqrt{cos^2(\theta_z) + cos^2(\delta) \cdot sin^2(\omega)} \tag{15}$$

Here, θ_z is zenith angle, δ is declination angle, and ω is hour angle. Finally, the heat removal factor is given by [36]:

$$F_R = \frac{\dot{m}_A \cdot c_{p,therminol}}{A_r \cdot U_L}\left[1 - \exp\left(-\frac{U_L \cdot F^{'} \cdot A_r}{\dot{m}_A \cdot c_{p,therminol}}\right)\right] \tag{16}$$

Here, $F^{'}$ is the collector efficiency factor and defined as [36]:

$$F^{'} = \frac{\frac{1}{U_L}}{\frac{1}{U_L} + \frac{D_{o,r}}{h_{fi} \cdot D_{i,r}} + \left(\frac{D_{o,r}}{2k} + ln\frac{D_{o,r}}{D_{i,r}}\right)} \tag{17}$$

where $D_{o,r}$ is the receiver outer diameter and $D_{i,r}$ is the inner diameter of the receiver. The power consumed in P-II is calculated as:

$$\dot{W}_{\mathrm{P-II}} = \frac{v\Delta P}{\eta_p} \tag{18}$$

where v, ΔP and η_P are the specific volume and pressure loss and pump efficiency, respectively. So, the exergy balance of *SF* is calculated as follows:

$$\dot{E}x_{d,SF} = \dot{E}x_{solar} + \dot{W}_{\mathrm{P-II}} + \dot{W}_{track} + \dot{m}_{A'}\psi_{A'} + \dot{m}_D\psi_D - \dot{m}_{B'}\psi_{B'} - \dot{m}_E\psi_E \tag{19}$$

Thermodynamic analysis of TES

The energy and exergy balances of *TES* are respectively given by:

$$\dot{m}_B h_B + \dot{m}_C h_C - \dot{m}_A h_A - \dot{m}_F h_F - \dot{Q}_{\mathrm{HE-I}} - \dot{Q}_{HST} - \dot{Q}_{\mathrm{CST}} + \dot{W}_{\mathrm{P-III}} + \dot{W}_{\mathrm{P-IV}} = 0 \tag{20}$$

$$\dot{E}x_{d,TES} = \begin{array}{l} \dot{m}_B(\psi_B - \psi_A) + \dot{m}_C(\psi_C - \psi_F) - \left(1 - \frac{T_0}{T_B}\right)\dot{Q}_{\mathrm{HE-I}} \\ -\left(1 - \frac{T_0}{T_E}\right)\dot{Q}_{l,HST} - \left(1 - \frac{T_0}{T_C}\right)\dot{Q}_{l,CST} + \dot{W}_{\mathrm{P-III}} + \dot{W}_{\mathrm{P-IV}} \end{array} \tag{21}$$

The energy balance of HE-I is given as:

$$\dot{Q}_{\mathrm{HE-I}} = \left(\dot{m}_B h_B - \dot{m}_A h_A\right) \cdot 0.98 - \left(\dot{m}_E h_E - \dot{m}_D h_D\right) \tag{22}$$

The energy modeling of the *HST* can be mainly analyzed in two stages including; charging and discharging. For the charging stage, the inlet heat of *HST* can be defined as [47]:

$$\dot{Q}_{HST} = \dot{Q}_E - \dot{Q}_{l,HST} \tag{23}$$

where $\dot{Q}_E$ is the heat energy obtained from the solar field at point E, and $\dot{Q}_{l,hst}$ is the lost heat from the storage tank during the charging period and calculated as follows:

$$\dot{Q}_{l,HST} = (UA)_{HST} \cdot (T_{HST} - T_{amb}) \tag{24}$$

where U and A are the overall heat transfer coefficient and heat transfer surface area of the storage tank, respectively. The overall heat transfer coefficient UA is a function of the volume of fluid in the tank and the tank loss coefficient per unit area (γ_{HL}), and is given by [48]:

$$UA = \gamma_{HL} \cdot \left(\frac{V}{H} + \pi \cdot D_t \cdot H\right) \tag{25}$$

where V and H are volume and height of the fluid in the tank and D_t are the diameter of the tank. The daily total heat gained is calculated as [47]:

$$\sum Q_{HST} = \dot{Q}_{HST} \cdot \Delta t \tag{26}$$

where Δt is the total time of charging which also means the insolation time (Δt_{ins}). The temperature in the *HST* can be calculated by:

$$T_{HST} = \frac{\sum Q_{HST}}{c_{p,HST} \cdot m_{HST}} \tag{27}$$

where m_{HST} is the total mass in the *HST*. For this stage, the change in the temperature of the *HST* can be calculated as [47]:

$$\Delta T_{HST} = T_{HST} - T^{+}_{HST} \tag{28}$$

$$T^{+}_{HST} = T_{HST} + \frac{\Delta t}{m_{HST} \cdot c_{p,HST}} \cdot (-(UA)_{HST} \cdot (T_{HST} - T_{amb})) \tag{29}$$

The total heat loss from *HST* during discharging is defined as:

$$Q_{HST,tlost} = m_{HST} \cdot c_{p,HST} \cdot \left(T_{HST} - T^{+}_{HST}\right) \tag{30}$$

For the discharging stage, the total heat transfer is defined as [47]:

$$Q_F = \sum Q_{HST} - Q_{HST,tlost} \tag{31}$$

where $\dot{Q}_F$ is the heat energy of molten salt at point F. The *CST* is also analyzed in the same way as the *HST*. At this time, the discharging process of *HST* means the charging of *CST*. So, the discharged heat (Q_D) in the *CST* is calculated as:

$$Q_D = \sum Q_{CST} - Q_{CST,tlost} \tag{32}$$

Thermodynamic analysis of PB

The energy and exergy balances of *PB* should be investigated in two stages including the direct and indirect working conditions. The direct condition includes working parameters when the *PB* is fed by PTC where the indirect one includes the parameters when *PB* is fed by *TES*. The energy balance equations for direct and indirect conditions are respectively given as:

$$\dot{m}_{B'} h_{B'} - \dot{m}_{A'} h_{A'} + \dot{m}_a h_a - \dot{m}_b h_b - \dot{Q}_{\mathrm{HE-III}} + \dot{W}_{\mathrm{P-I}} - \dot{W}_{\mathrm{G}} = 0 \tag{33}$$

$$\dot{m}_F h_F - \dot{m}_C h_C + \dot{m}_a h_a - \dot{m}_b h_b - \dot{Q}_{\mathrm{HE-II}} + \dot{W}_{\mathrm{P-I}} - \dot{W}_{\mathrm{G}} = 0 \tag{34}$$

Here, mass rates of the flow in *ORC* are calculated according to working times of Δt_{ins} and $24 - \Delta t_{ins}$ for direct and indirect cases, respectively. According to the energy balance equations, the exergy balances for the direct and indirect working conditions are respectively given as:

$$\dot{E}x_{d,PB-direct} = \dot{m}_{B'}\psi_{B'} - \dot{m}_{A'}\psi_{A'} + \dot{m}_a\psi h_a - \dot{m}_b\psi_b - \left(1 - \frac{T_0}{T_{B'}}\right)\dot{Q}_{\mathrm{HE-III}} + \dot{W}_{\mathrm{P-I}} - \dot{W}_{\mathrm{G}} \tag{35}$$

$$\dot{E}x_{d,PB-indirect} = \dot{m}_F\psi_F - \dot{m}_C\psi_C + \dot{m}_a\psi_a - \dot{m}_b\psi_b - \left(1 - \frac{T_0}{T_F}\right)\dot{Q}_{\mathrm{HE-I}} + \dot{W}_{\mathrm{P-I}} - \dot{W}_{\mathrm{G}} \tag{36}$$

The generated power; $\dot{W}_G$ is calculated as:

$$\dot{W}_G = \eta_G \cdot \dot{W}_T \tag{37}$$

where $\eta_G$is the generator efficiency and taken as 97% for the calculations. $\dot{W}_T$ is the power obtained from the turbine and given as:

$$\dot{W}_T = \dot{m}_{wf} \cdot (h_3 - h_4) \tag{38}$$

Here, $\dot{m}_{wf}$ is the mass flow of the working fluid of *ORC*. Therefore, the net electric power of the generator is:

$$\dot{W}_{net} = \dot{W}_G - \dot{W}_{P-I} - \dot{W}_{P-II} - \dot{W}_{P-III} - \dot{W}_{P-IV} - \dot{W}_C - \dot{W}_{track} \tag{39}$$

where $\dot{W}_{P-I}$ $\dot{W}_{P-II}$, $\dot{W}_{P-III}$, $\dot{W}_{P-IV}$, $\dot{W}_C$ and $\dot{W}_{track}$ are respectively required powers of P-I, P-II, P-III, P-IV, fan, and tracking system (assumed as 35 W per collector). Besides, the parasitic losses were included as 2% [49].

Economic analysis

The Net Present Value (*NPV*) method is used in the economic analysis of the system. In this method, the cash flows of the project invested are determined by taking the time value of money into account. The lifetime of power plant was taken as 20 years in this study. If *NPV* is negative, then the project is not investable even though it gains ground during the lifetime of the system. *NPV* method can be expressed mathematically as follows [50]:

$$NPV = \sum_{t=0}^{n} \frac{B_t}{(1+r)^t} \tag{40}$$

where n is the lifetime of the system, B_t is cash flow in t^{th} year. r is the discount rate and was concluded into calculations with an expectation of a profit margin of 10%. B_t value is calculated by the following equation for the proposed system:

$$B_t = C_{elec} - C_{mr} - C_{per} \tag{41}$$

where $C_{elec}$is the gain of electricity. C_{mr} is the cost of maintenance and repair, C_{per} is the total annual personnel expenses. For the cost analysis of the designed system, the cost of the initial investment, the operating cost, and the salvage cost were taken into consideration. The investment cost of the system (C_{inv}) consists of the cost of the solar field (C_{SF}), the cost of the thermal energy storage system (C_{TES}), and the cost of the power block (C_{PB}), and is given by:

$$C_{inv} = C_{SF} + C_{TES} + C_{PB} \tag{42}$$

C_{SF} and C_{PB} values were concluded as a whole and taken as 6000 US $/kW$_e$ [51]. C_{TES} was concluded as 25.68 US$/kWh$_{th}$ [52]. Taking the salvage cost of the system (C_{sal}) into consideration, the initial cost of the system is calculated as:

$$C_{init} = C_{inv} - C_{sal} \tag{43}$$

The salvage cost of the plant was taken as 10% of the investment cost. The cost of maintenance and repair of the system was taken as 2% of the investment cost [50]. The labor force requirement of the power plant was included in calculations by considering 1 engineer and 10 workers. The minimum wage of 2019 was taken into account for the calculations as 485.46 $. According to this, the total annual personnel expense is given as:

$$C_p = 485.46 \cdot 12 \cdot (2.1 \cdot 1 + 1.2 \cdot 10) \tag{44}$$

Depending on the financial incentive of the government on renewable sources, the unit cost of electricity was included in calculations as 0.133 $/kWh for the first 10 years, and it was taken as 0.077 $/kWh [53]. Accordingly, the benefit of electricity is given as:

$$C_{elec} = \dot{W}_{net} \cdot c_{elec} \begin{cases} c_{elec} = 0.133; for the first 10 years \\ c_{elec} = 0.077; for the last 10 years \end{cases} \tag{45}$$

Optimization procedure

The negative *NPV* commentates the designed systems are not investable although the system is profitable. This means the designed system has a long payback period and it would be more attractive to evaluate the investment cost in a different financial area. Therefore, to decide on the investment, the *NPV* values should be higher as much as they could be. In this regard, the optimum working conditions are determined according to the *NPV* values of the system as an objective function. The economic evaluation is structured on the idea of the installation of maximum power generation capacity of the organic turbine on daily basis. It means that the economic values are calculated on yearly basis according to the related maximum daily value of the whole system, and the *NPV* is then calculated for the life cycle of the system considering the daily net power output values. The optimum system is determined as the one with the highest *NPV* value. Optimal points were determined concurrently since all the parameters have been affected by each other. In this aim, an excel code was formed to obtain the results of the parametric evaluation.

Results and discussion

The handled system adapted for the low-radiation zone is evaluated block by block to obtain the optimal system. As the first step, *PB* is evaluated to find the best *ORC* configuration. As the second step, the *TES* side is evaluated taking *SF* and the best configuration of *PB* into account. At this step, the analyses are conducted within the limits of the molten salts. Finally, *SF* is evaluated taking the best configuration of both *PB* and *TES*.

Optimization of PB

The maximum value of the *TES* and *PB* (installed capacity) on daily basis is handled for the installation of the system, and *NPV* of any design is conducted on yearly basis considering this maximum. The effects of the temperature and pressure at the turbine inlet are simultaneously investigated where the outlet temperature is set to 56 °C as mentioned in section 3.3. The outlet pressure of the turbine is determined according to the saturation values of the handled working fluids. The values of *SF* and *TES* were selected as available extremes (T_A = 110 °C, T_B = 400 °C, T_D = 100 °C, and T_E = 390 °C) values taking the assumed temperature difference, the maximum working temperature, and melting temperature into consideration. The results are given in Figs. 5–11.

According to Fig. 5, the range of P_3 was investigated between 2000 kPa and 10000 kPa covering the subcritical and supercritical cycles where T_3 was investigated between 180 °C and the available highest temperature of 380 °C. The driving parameter is the pressure in this case. The optimum pressure for the highest *NPV* was determined as 8000 kPa where the optimum temperature was determined as the maximum available temperature of 380 °C. The maximum temperature was determined taking a temperature difference of 10 °C. In this case, the best cycle is the supercritical one with an *NPV* of −39.72 million US$.

According to Fig. 6, the range of P_3 was investigated between 2000 kPa and 6000 kPa covering the subcritical and supercritical cycles where T_3 was investigated between 140 °C and the available highest temperature of 380 °C. The driving parameter is also the pressure in this case

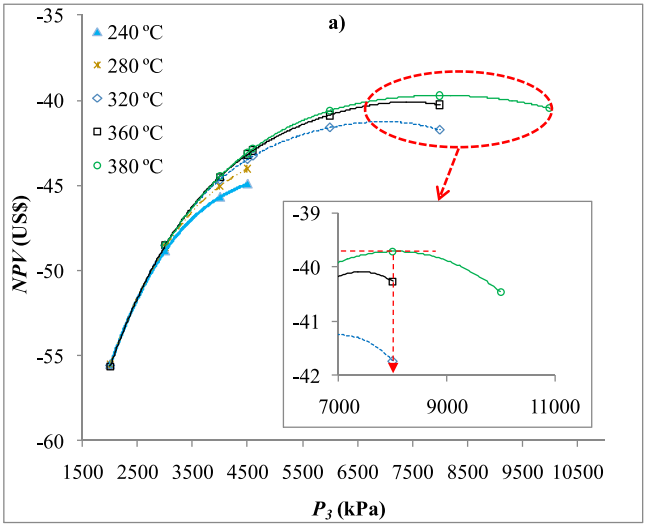

Fig. 5. *NPV* variation vs. P_3 (a) and T_3 (b) for R152a.

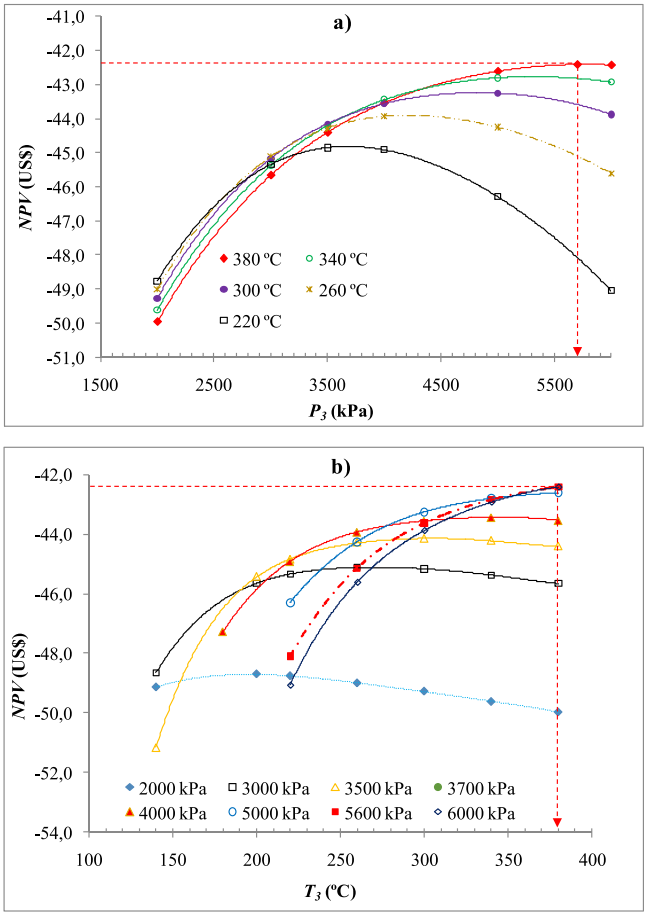

Fig. 6. *NPV* variation vs. P_3 (a) and T_3 (b) for R600a.

although both the pressure and temperature have collective effects at the lower pressures (<5600 kPa). Thus, the optimum pressure was determined as 5700 kPa where the optimum temperature was determined as the maximum available temperature of 380 °C. In this case, the best cycle is the supercritical one with an *NPV* of −42.41 million US$.

According to Fig. 7, the range of P_3 was investigated between 2000 kPa and 6000 kPa covering the subcritical and supercritical cycles where T_3 was investigated between 160 °C and the available highest temperature of 380 °C. Both the pressure and temperature have collective effects as the driving parameters in this case. The optimum pressure was determined as 4000 kPa where the optimum temperature was determined as 300 °C. In this case, the best cycle is the subcritical one with an *NPV* of –32.96 million US$.

According to Fig. 8, the range of P_3 was investigated between 1500 kPa and 6000 kPa where T_3 was investigated between 200 °C and the available highest temperature of 380 °C. Both the pressure and temperature have collective effects as the driving parameters in this case. Therefore, the optimum pressure was determined as 4750 kPa where the optimum temperature was determined as 333 °C. In this case, the best cycle is the supercritical one with an *NPV* of −19.13 million US$.

According to Fig. 9, the range of P_3 was investigated between 1800 kPa and 4500 kPa where T_3 was investigated between 230 °C and the available highest temperature of 380 °C. Both the pressure and temperature have collective effects as the driving parameters in this case. The optimum pressure was determined as 2950 kPa where the optimum temperature was determined as 270 °C. In this case, the best cycle is the subcritical one with an *NPV* of −15.30 million US$.

According to Fig. 10, the range of P_3 was investigated between 2000 kPa and 4200 kPa where T_3 was investigated between 280 °C and the available highest temperature of 380 °C. Both the pressure and

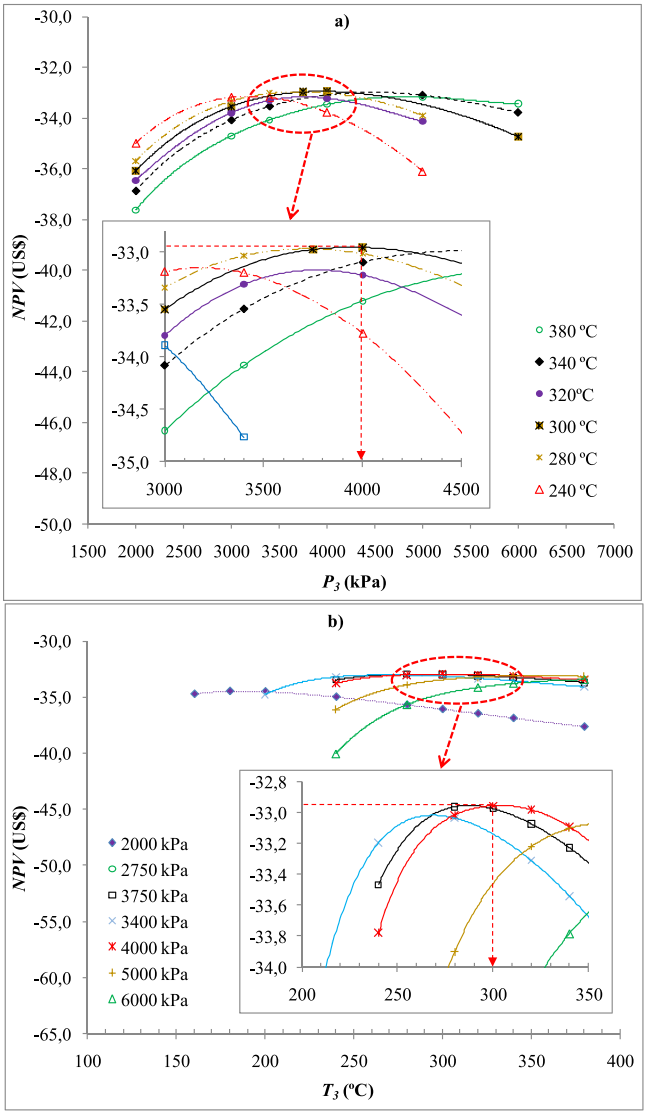

Fig. 7. *NPV* variation vs. P_3 (a) and T_3 (b) for R601a.

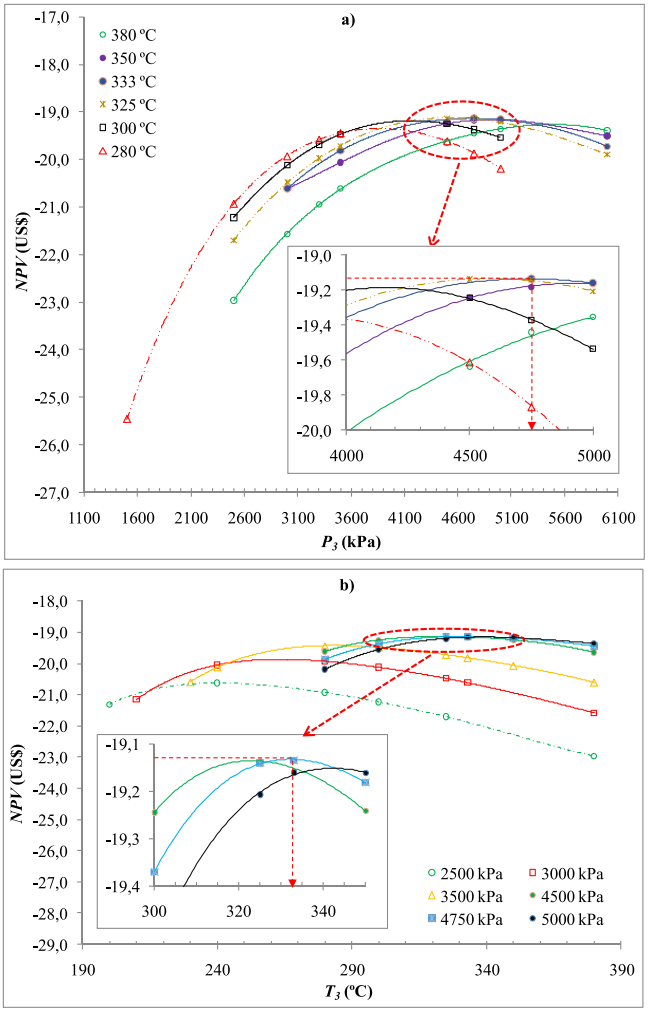

Fig. 8. *NPV* variation vs. P_3 (a) and T_3 (b) for cyclopentane.

temperature have collective effects as the driving parameters in this case. The optimum pressure was determined as 3500 kPa where the optimum temperature was determined as 345 °C. In this case, the best cycle is the subcritical one with an *NPV* of −5.61 million US$.

In Fig. 11, the CRC power plant was evaluated. The range of P_3 was investigated between 300 kPa and 3265 kPa where T_3 was investigated between 200 °C and the available highest temperature of 380 °C. Both the pressure and temperature have collective effects as the driving parameters in this case. The maximum available pressure was determined according to the dryness fraction at the outlet of the turbine that was assumed 0.9 as a minimum. Therefore, the optimum pressure was determined as 3265 kPa where the optimum temperature was determined as 380 °C. The maximum limit values were determined as the optimum point for this case. In this case, the best cycle is the subcritical one with an *NPV* of 9.01 million US$.

According to optimized results, the best design was determined as *CRC*. The *ORC* designs were found nonprofitable for any case. The main cause of this situation is the outlet condition of the condenser since it is limited by the ambient temperature of Bilecik depending on the air-cooling. Henceforth, the outlet temperatures of the fluids are relatively higher which means there is still possible useful energy that can be evaluated.

Optimization of TES

Taking the optimum point of *PB* and extreme points of *SF* into account, the *TES* side of the system was investigated for R718. The other fluids were not included since they have a similar trend. The *NPV* variations versus T_D and T_E are given in Fig. 12.

According to Fig. 12, as expected, the *NPV* decreases with the increase of T_D. The minimum temperature of T_D is handled as 100 °C taking the melting temperature of molten salt (99 °C) and the temperature decrease of *CST* occurred by the heat losses into account. However, for every single increase of 10 °C considering the minimum temperature of 10 °C HE-I, the variation of *NPV* is about 1.66%-2.71%. It means relatively a lower impact on the design; therefore, the different integrated usages could be available according to the need for the region. Also as expected, the *NPV* increases with the increase of T_E. The maximum temperature of T_E is handled as 390 °C taking the maximum stable working temperature of heat transfer fluid (400 °C). For every single increase of 10 °C considering a temperature difference of 10 °C in HE-I, the variation of *NPV* is about 0.64%-1.44% which also means a relatively lower impact on the design. For the constant temperature of $T_E = 400$ °C, this increase is about 0.41%-0.84%. For the final decision, the optimum point is determined as the maximum available of 390 °C for T_E where it is determined as the minimum available of 100 °C for T_D.

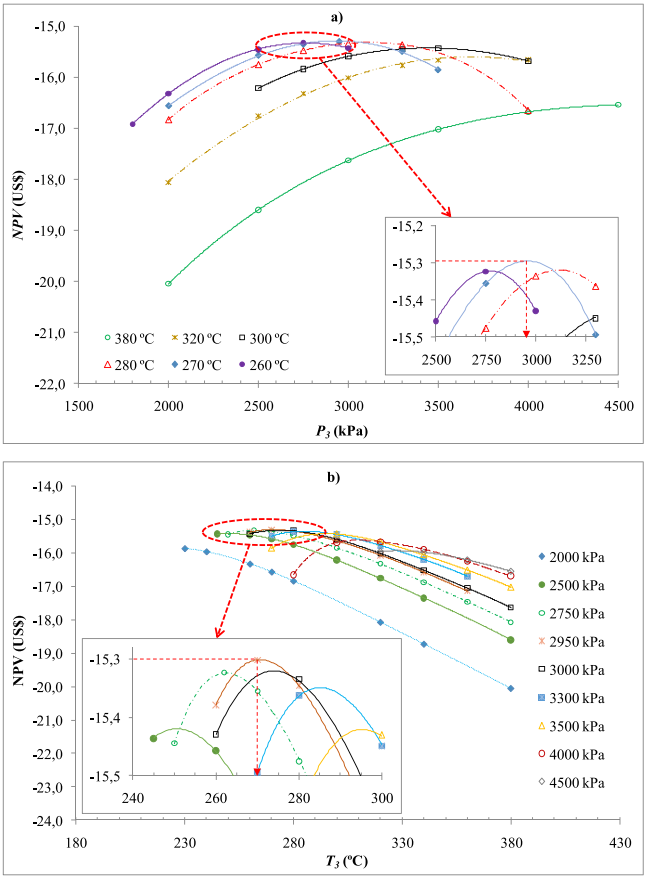

Fig. 9. *NPV* variation vs. P_3 (a) and T_3 (b) for cyclohexane.

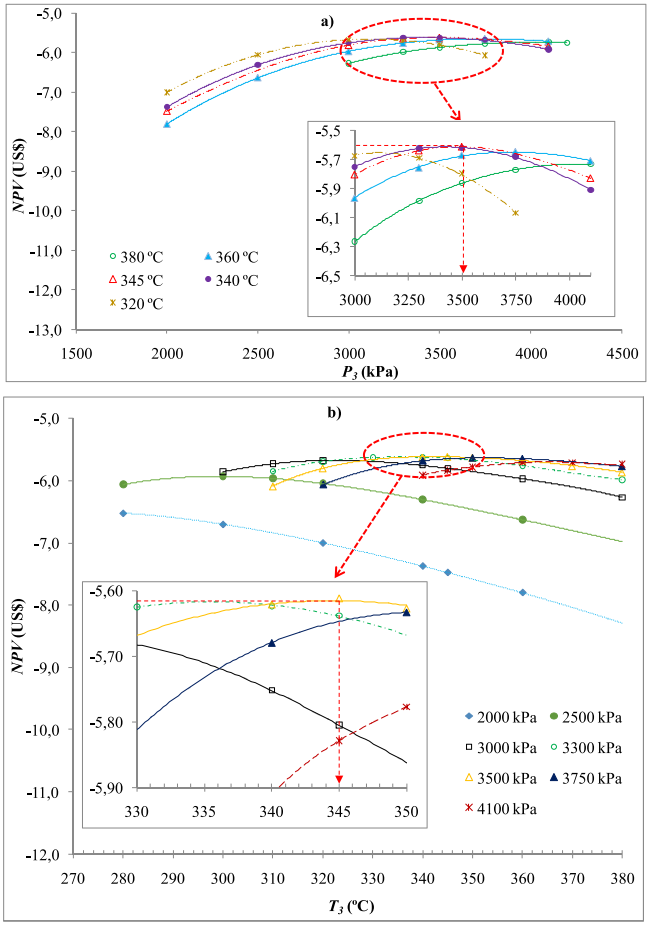

Fig. 10. *NPV* variation vs. P_3 (a) and T_3 (b) for toluene.

Optimization of SF

Taking the optimum point of *PB* and extreme points of *TES* into account, the *SF* side of the system was investigated for the variations of x, T_A, and T_B. The variation of *NPV* versus x is given in Fig. 13.

According to Fig. 13, *NPV* increases up to a certain point, and then it decreases with the increase of mass ratio. It shows that there is a maximum peak point and it means this point is the optimal one for the investment. The optimal mass ratio is determined as 34.1%. The optimal point is not affected by the kind of working fluid or the working parameters of the handled system. The single issue that affects the optimal point is just the solar irradiation characteristics of the region. Therefore, this effect is one of the most critical ones that should be taken into account for any solar area. The *NPV* variation versus T_A and T_B is given in Fig. 14.

According to Fig. 14, the *NPV* decreases with the increase of T_A. The minimum temperature of T_A is handled as 110 °C taking a temperature difference of 10 °C in HE-I into account. For every single increase of 10 °C considering a temperature difference of 10 °C in HE-II, the variation of *NPV* is about 0.88%–1.02%. For every single increase of 10 °C in T_B considering a temperature difference of 10 °C in HE-I, the increase of *NPV* is about 0.64%–1.44%. For the final decision, the optimum point is determined as the maximum available of 400 °C for T_B where it is determined as the minimum available of 110 °C for T_A.

Overview of the optimal designs

The optimal points were determined as the maximum or minimum available ones for T_A, T_B, T_D, T_E. The optimal points of other points are variable depending on the fluids. The optimal characteristics of the system are summarized in Table 4. The optimum points were obtained for the supercritical cycle in the case of using R152a, R600a, R601a, and cyclopentane where these points were obtained for the subcritical cycle for the other working fluids. Any of the working fluids (except for R718) is not profitable for the low-radiation zone. The best and sole choice is R718 with an *NPV* value of 9.012 million US$ and a payback period of 8.9 years. The maximum energy and exergy efficiencies for this case are respectively calculated as 11.05% and 11.86% with an installed turbine capacity of 22.20 MW. The produced electricity generation is recorded as 365,756.7 GJ per year. The minimum required *PTC* numbers were calculated as well and were recorded as 2772 for R718. This means the suitable areas with a minimum surface area of 451,559 m^2 are profitable for the investment. For the other fluids, the turbine outlet pressure is relatively higher which means a higher outlet temperature. Therefore, there is still potential to be evaluated on a remarkable scale.

Thermodynamic evaluation of the optimal system

Thermodynamic evaluations were conducted for the optimal values of R718. Considering the daily dynamic evaluation, the design point was determined as the one with the required maximum turbine installation capacity and required *TES* volume. In this aim, energy efficiency (η), exergy efficiency (ε), net yearly electricity generation (E_{net}), available installed power capacities (W_T), and net power out (W_{net}) were determined. The variation of net electricity generation, installed capacity, and net power output is given in Fig. 15.

According to Fig. 15, the available installed capacity of the system ranges between 13.44 MW and 22.20 MW. The maximum calculated installation capacity is 22.202 MW and 22.196 MW for the direct feed and the *TES* feed, respectively. The maximum available installed power capacity is obtained for the 191st day of the year (July 10th) with an

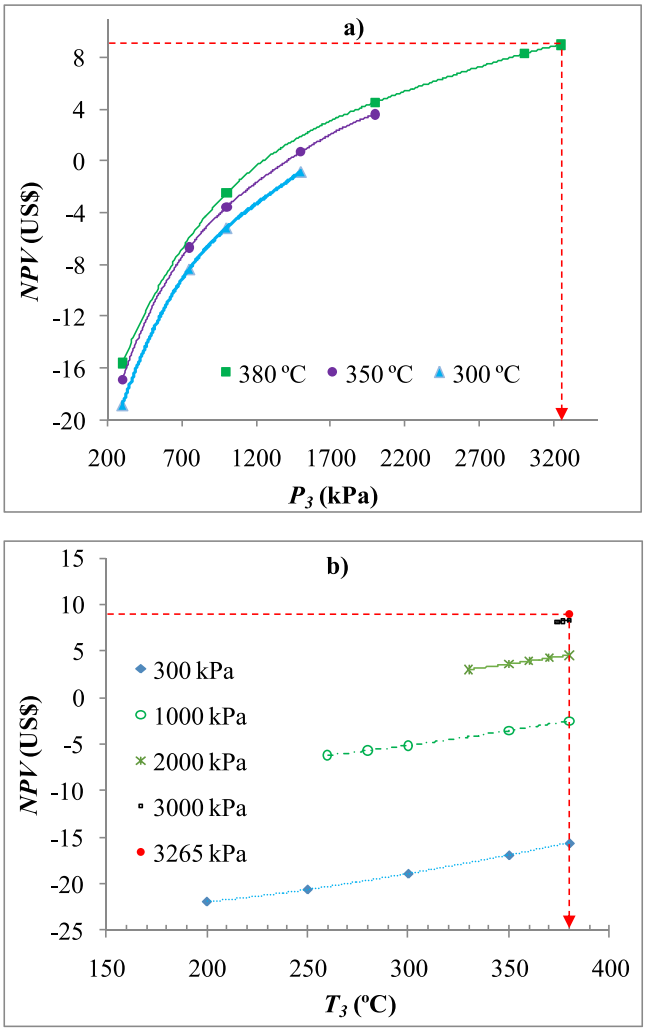

Fig. 11. *NPV* variation vs. P_3 (a) and T_3 (b) for R718.

insolation time of 10.52 h and *TES* working time of 13.48 h. Therefore, the installed capacity is determined as the maximum requirement of 22.2 MW. The auxiliary power requirement ranges between 1.34 MW and 2.73 MW. The electricity generation rate ranges between 482,625.50 MWh and 1,500,363.05 MWh, which generates a yearly total of 365,756,712.15 MJ. The variation of energy and exergy efficiencies is given in Fig. 16.

According to Fig. 16, η values of the optimal design range between 9.94% and 11.05%, where ε values range between 22.89% and 23.32%. At the design point, η and ε are determined as 10.19% and 10.94%, respectively. The variations of the heat loads and heat losses of *TES* are given in Fig. 17.

According to Fig. 17, the stored heat ranges between 3,515,845.19 MJ and 11,406,904.63 MJ for *HST*, and range between 1,978,342.20 and 6,418,587.63 MJ for *CST*. The heat losses range between 30,644.65 MJ and 95,264.59 MJ for *HST*, and range between 7,773.41 MJ and 21,738.63 MJ for *CST*. The design point is determined as the 172nd day of the year (June 21st). The maximum heat loss that occurred in *HST* is about 0.88% where it is about 0.42% for *CST*. The variation of temperature decrease depending on the heat losses is given in Fig. 18.

According to Fig. 18, depending on the ambient conditions, the temperature decrease ranges between 5.53 °C and 5.96 °C for *HST* where it ranges between 1.13 °C and 1.55 °C for *CST*. Taking the design point of the system into consideration, the technical energy and exergy analysis results of the optimum system are given in Table 5.

According to Table 5, the minimum exergy efficiency is determined for the condenser as 16.56% although it has higher energy efficiency. The exergy efficiency of the *SF* (PTC) is obtained as 34.71%, and this value is agreeable to that of Ref. [54]. The exergy efficiency of *TES* is calculated as 65.94%, which is agreeable to that of Ref. [55]. The exergy efficiency of *PB* is calculated as 41.56%, and it is agreeable to the literature values [56]. The exergy efficiency of the overall system was

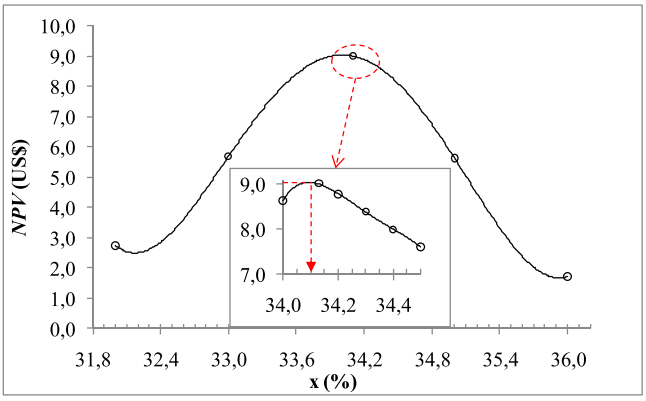

Fig. 13. *NPV* variation vs. mass fraction (x) of heat transfer fluid.

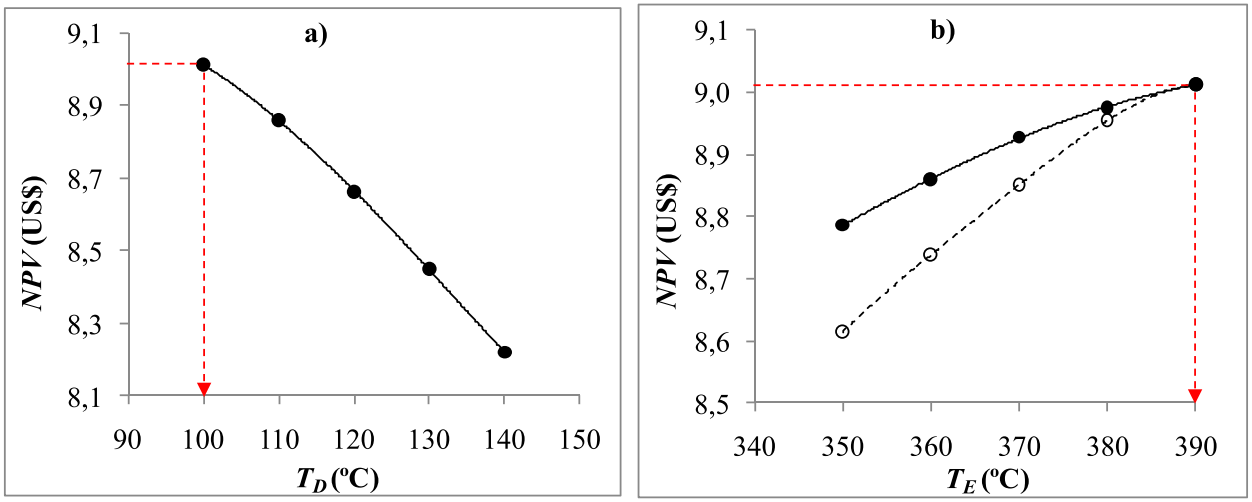

Fig. 12. *NPV* variation vs. T_D (a) and T_E (b).

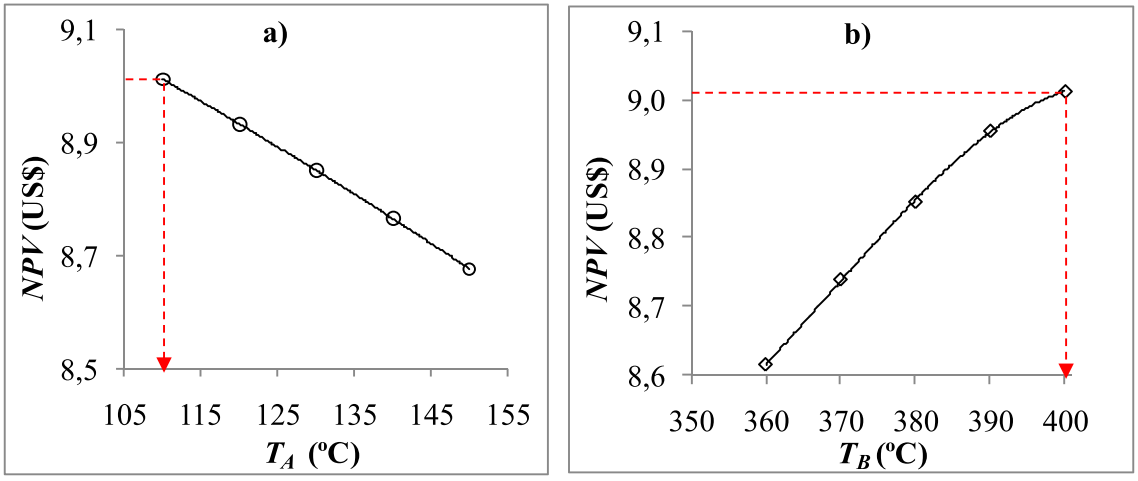

Fig. 14. *NPV* variation vs. T_A (a) and T_B (b).

Table 4
Optimal characteristics of the system for the selected fluids.

Property	R152a	R600a	R601a	Cyclopentane	Cyclohexane	Toluene	R718
T_A (°C)	110						
T_B (°C)	400						
T_D (°C)	100						
T_E (°C)	390						
T_1 (°C)	56						
ORC type	Supercritical	Supercritical	Supercritical	Supercritical	Subcritical	Subcritical	Subcritical
P_1 (kPa)	1364.300	791.560	244.320	125.860	45.098	15.784	16.533
T_2 (°C)	62.20	60.32	58.34	58.47	57.34	56.26	56.33
P_2 (kPa)	9163	5816	4082	4847	3010	3571	3316
T_3 (°C)	380	380	300	333	270	345	380
P_3 (kPa)	8000	5700	4000	4750	2950	3500	3250
T_4 (°C)	297.35	322.53	232.68	206.44	188.74	206.53	56.43
P_4 (kPa)	1392.140	807.714	249.306	128.429	45.098	16.106	16.870
η_{max} (%)	4.92	3.99	5.33	7.57	7.84	9.34	11.05
ε_{max} (%)	5.28	4.29	5.73	8.12	8.42	10.03	11.86
$\dot{W}_{T,max}$ (MW)	12.56	10.42	12.70	16.79	16.98	19.66	22.20
$\dot{W}_{net,max}$ (MW)	8.28	6.41	8.90	13.15	13.58	16.40	19.47
E_{net} (GJ/y)	151,202.9	118,751.4	165,608.7	243,875.7	253,456.3	305,917.4	365,756.7
NPV (million US$)	−39.718	−42.406	−32.955	−19.135	−15.302	−5.612	9.012
Payback period (year)	14.5	16.2	13.2	10.6	10.1	9.6	8.9
Minimum PTC number	–	–	–	–	–	–	2772

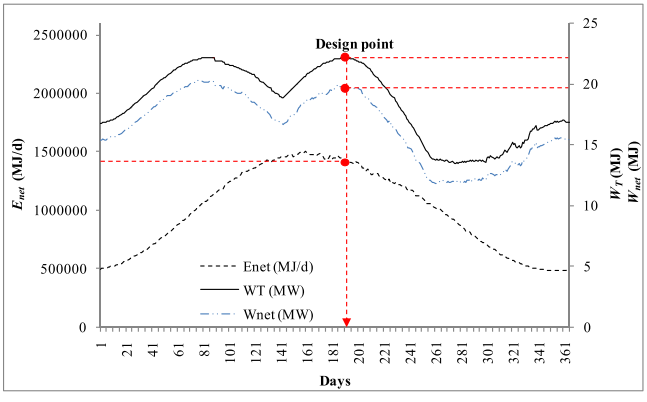

Fig. 15. The variation of E_{net}, W_T, and W_{net} for the optimal points of R718.

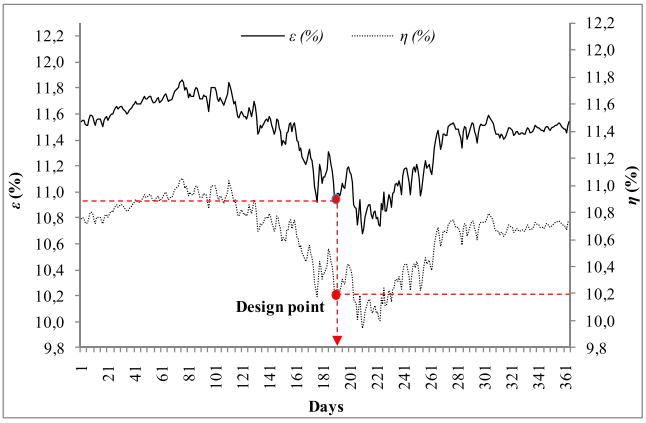

Fig. 16. The variation of η and ε.

calculated as 10.94%, which is relatively lower in comparison to those of literature [57]. The main cause, depending on the air cooling system, is the higher temperature value at the outlet of the condenser.

Environmental evaluation of optimal designs

Depending on the geographical location, the electricity need of

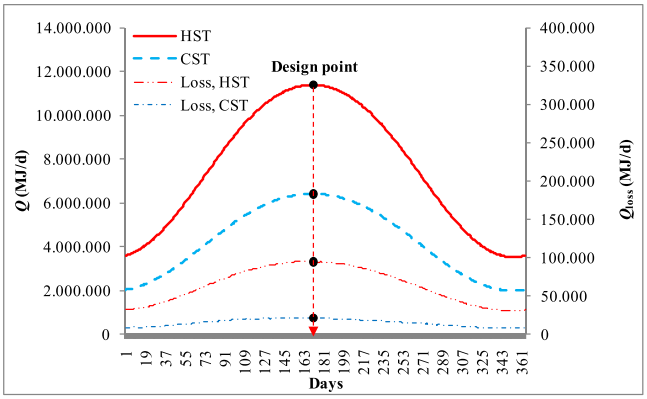

Fig. 17. Daily heat loads for *TES*.

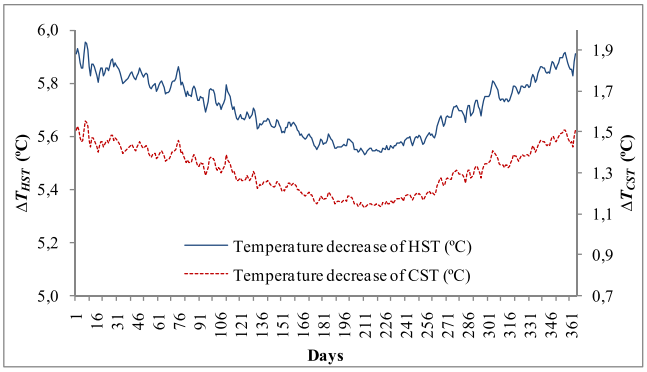

Fig. 18. Variation of the temperature decrease for *HST* and *CST*.

Bilecik province is satisfied by the coal-fired power plant located in Kutahya that is the nearest city and grid network. It means that a power plant driven by renewable energy sources would decrease the load of this coal-fired power plant. So, the emissions released into the atmosphere would also decrease since lignite with low energy value and high sulfur content is used in this plant. In this aim, taking the technical properties of this coal-fired power plant into account [58,59], the reduction of the related emission contents is given as in Table 6.

The other concern of environmental management is not to have a strong regulation on these emission releases. Although there are some penal sanctions on this issue, it does not solve the problem because of the energy requirement. In this regard, a carbon tax would be an appropriate solution. However, at this time, it would bring new concerns amongst the consumers, producers, and commissioners. Although renewable energy comes into prominence as the strongest solution in this way, the entrepreneurs keep away from the investments because of higher costs. Turkey applies an encouragement politic to disseminate the solar applications that guarantee to purchase the generated electricity for the first 10 years. As seen from the results of this study, it is not sufficient for many cases. In this regard, a tax discount or a carbon tax on the sale price would be an attractive solution. However, it should be deeply argued on the amount of this tax. Assuming a carbon tax ranging between 5% and 18%, the re-calculated values of *NPV* and payback periods are also given in Table 6. According to Table 6, it is available to prevent CO_2, SO_2, and NO_x emissions in an amount of 108,046.4, 2,457.6, and 249.7 gross tons per year. The investment is not profitable for R152a, R600a, R601a, and cyclopentane in any case of tax discount. The investment is profitable for cyclohexane if a discount of 15% is applied. The investment for toluene is profitable if a discount of 5% is applied.

Conclusion

For the low-radiation zone with a DNI value of ranging between 241 and 398 W/m^2, the *ORC* power plant driven by *PTC* was analyzed from the energy, exergy, economics, and environmental points of view. The

Table 5
Exergy analysis results of the best investable design.

Component		E_i (MJ/d)	E_o(MJ/d)	Q (MJ/d)	W (MJ/d)	Ex_i (MJ/d)	Ex_o(MJ/d)	Ex_d (MJ/d)	η (%)	Ɛ (%)
SF	PTC	13,838,702.7	7,602,118.9	−6,206,328.8	30,255.0	12,862,045.6	4,475,200.8	8,417,099.8	54.81	34.71
TES	HE-I	5,007,515.7	4,907,365.4	−100,150.3	–	2,947,814.8	2,006,225.2	885,797.6	98.00	69.95
	HST	11,221,790.9	11,129,217.8	−92,573.1	5,309.3	2,143,292.7	2,091,732.8	107,646.7	99.13	94.98
	CST	6,334,235.6	6,314,425.5	−19,810.0	2,654.7	141,013.6	137,067.4	10,606.9	99.65	92.48
	Overall	5,007,515.7	4,794,982.2	−112,383.2	7,964.0	2,947,814.8	1,950,719.2	1,004,051.2	95.60	65.94
PB	HE-II	4,814,792.3	4,718,496.4	−96,295.8	–	1,950,719.2	1,836,229.3	73,840.2	98.00	96.21
	HE-III	2,594,603.2	2,542,711.1	−51,892.1	–	1,527,386.0	989,510.3	515,277.7	98.00	66.26
	T/G	7,850,054.1	5,838,558.0	−353,017.6	−1,658,478.6	2,849,775.1	517,134.2	812,975.1	82.45	71.47
	C	5,260,044.6	5,154,843.7	−305,112.6	199,911.7	529,842.0	120,833.8	608,919.9	94.41	16.56
	P-I	578,513.4	588,846.6	−2,583.3	12,916.5	15,585.7	24,035.5	5,637.2	80.00	80.22
	Overall	7,409,395.5	588,846.6	−808,901.4	−1,445,650.3	3,478,105.3	156,632.4	2,016,650.1	19.51	41.56
Overall System		13,808,447.7	5,154,843.7	−7,127,613.4	−1,407,431.3	12,862,045.6	120,833.8	7,934,218.0	10.19	10.94

*P-II is counted in *SF*, **P-III is counted in HST, ***P-IV is counted in CST.

Table 6
Emission reduction and economic evaluation including a carbon tax.

Property	Discount (%)	R152a	R600a	R601a	Cyclopentane	Cyclohexane	Toluene	R718
CO_2 (10^3 ton/y)	–	44,666.1	35,079.8	48,921.6	72,042.1	74,857.8	90,369,5	108,046.4
SO_2 (10^3 ton/y)	–	1,016.0	797.9	1112.8	1,638.7	1,702.7	2,55.6	2,457.6
NO_x (10^3 ton/y)	–	103.2	81.1	113.1	166.5	173.0	208.9	249.7
NPV (million US$)	5	−36.553	−39.921	−29.489	−14.031	−9.999	0.790	16.667
Payback period (year)		13.9	15.5	12.8	10.6	9.8	9.3	8.8
NPV (million US$)	10	−33.389	−37.436	−26.023	−8.927	−4.695	7.193	24.301
Payback period (year)		13.4	15.0	12.3	9.8	9.6	9.1	8.6
NPV (million US$)	15	−30.224	−34.951	−22.557	−3.823	0.608	13.595	31.976
Payback period (year)		12.9	14.5	11.8	9.6	9.4	8.9	8.4
NPV (million US$)	18	−29.326	−33.460	−20.477	−0.761	3.790	17.436	36.569
Payback period (year)		12.6	14.2	11.5	9.5	9.3	8.8	8.3

system was concurrently optimized taking the *NPV* values as an objective function for making a decision of system applicability. Six different environment-friendly working fluids were performed for the proposed system. The conventional steam Rankine (*CRC*) cycle with R718 was also performed. The following issues were concluded:

- The optimum design with the highest *NPV* was determined as the conventional Rankine cycle (*CRC*) with R718. The optimal energy and exergy efficiencies of *CRC* were respectively calculated as 10.19% and 10.94% where the maximum energy and exergy efficiencies were calculated as 11.05% and 11.86%.
- The *NPV* value of the optimal power plant was calculated as 9.012 million US$ with an installed capacity of 22.20 MWe and a net capacity of 19.47 MWe, which means the system was profitable for the investment. The yearly net electricity generation was calculated as 365,756.7 GJ/y.
- The optimal points were determined when T_A, T_B, T_D, T_E, T_2, and P_3 are 110 °C, 400 °C, 100 °C, 390 °C, 380 °C, and 3250 kPa, respectively.
- For the optimal case, it was determined that the reduction of 108,046.4 ktones, 2,457.6 ktones, and 249.7 ktones were available in the emissions of CO_2, SO_2, and NO_x, respectively.
- The *ORC* designs were found not investable for the low-radiation zone. In this regard, different energy policies on the financial issues of the government were introduced from the environmental point of view. Thus, a suitable way was offered on the environmental tax including the discount of value-added tax or a new carbon tax ranging between 5% and 18%. The *ORC* with toluene was found investable when a discount or tax of about 5% was applied. The *ORC* with cyclohexane was found investable when this rate was applied as 15%.

Future studies

Since the efficiency values of cases using refrigerants are relatively low depending on the higher temperature at the outlet of the turbine, a common application-which an internal heat exchanger is used- can be used to improve the energy and exergy efficiencies. Nevertheless, it is not expected that this application would be investable for the selected fluids except for toluene. Thereby, the most convenient choice seems to be the application including one or more bottoming cycles. In this regard, the R718 steam cycle should be designed as the bottoming cycle depending on its conditions at the turbine outlet since it enables us to catch the maximum available points. Therefore, the two-staged cycles of R152a/R718 and R600a/R718 can be taken into consideration. Three staged cycles of R600a/Cyclopentane/R718 and R152a/Cyclohexane/R718 can also be taken into consideration.

CRediT authorship contribution statement

Oguz Arslan: Conceptualization, Methodology, Validation, Writing - review & editing, Investigation, Supervision. **Damla Kilic:** Data curation, Investigation, Resources.

Declaration of Competing Interest

The authors declare that they have no known competing financial interests or personal relationships that could have appeared to influence the work reported in this paper.

References

[1] Javadi MA, Ahmadi MH, Khalaji M. Exergetic, economic, and environmental analyses of combined cooling and power plants with parabolic solar collector. Environ Prog Sustainable Energy 2020;39:e13322.
[2] Grosu L, Mathieu A, Feidt M, Ahmadi MH, Sadeghzadeh M. Steady state operation exergy-based optimization for solar thermal collectors. Environ Prog Sustainable Energy 2020;39:e13359.
[3] Vakilabadi MA, Bidi M, Najafi AF, Ahmadi MH. Energy, exergy analysis and performance evaluation of a vacuum evaporator for solar thermal power plant zero liquid discharge systems. J Therm Anal Calorim 2020;139:1275–90.
[4] Zhang C, Liu C, Xu X, Li Q, Wang Z, Chen X. Effects of superheat and internal heat exchanger on thermo-economic performance of organic Rankine cycle based on fluid type and heat sources. Energy 2018;159:482–95.
[5] Wand D, Dai X, Wu Z, Zhao W, Wang P, Hu B, et al. Design and testing of a 340 kW organic rankine cycle system for low pressure saturated steam heat source. Energy 2020;210:118380.
[6] Ozahi E, Tozlu A, Abusoglu A. Thermoeconomic multi-objective optimization of an organic Rankine cycle (ORC) adapted to an existing solid waste power plant. Energy Convers Manage 2018;168:308–19.
[7] Gao X, Gu Q, Ma J, Zeng Y. MVR heat pump distillation coupled with ORC process for separating a benzene-toluene mixture. Energy 2018;143:658–65.
[8] Abrosimov KA, Baccioli A, Bischi A. Techno-economic analysis of combined inverted Brayton-Organic Rankine cycle for high-temperature waste heat recovery. Energy Convers Manage 2020;207:112336.
[9] Arslan O, Ozgur MA, Kose R. Electricity generation ability of the Simav geothermal field: a technoeconomic approach. Energy Sources Part A 2012;34:1130–44.
[10] Moloney F, Almatrafi E, Goswami DY. Working fluid parametric analysis for recuperative supercritical organic Rankine cycles for medium geothermal reservoir temperatures. Renewable Energy 2020;2020(147):2874–81.
[11] Mokarram NH, Mosaffa AH. Investigation of the thermoeconomic improvement of integrating enhanced geothermal single flash with transcritical organic Rankine cycle. Energy Convers Manage 2020;2020(213):112831.
[12] Yadav K, Sircar A. Selection of working fluid for low enthalpy heat source Organic Rankine Cycle in Dholera, Gujarat, India. Case Stud Thermal Eng 2019;16:100553.
[13] Noroozian A, Naeimi A, Bidi M, Ahmadi MH. Exergoeconomic comparison and optimization of organic Rankine cycle, trilateral Rankine cycle and transcritical carbon dioxide cycle for heat recovery of low-temperature geothermal water. Proc Institution Mech EngPart A: J Power Energy 2019;233:1068–84.
[14] Wang N, Zhang S, Fei Z, Zhang W, Shao L, Sardari F. Thermodynamic performance analysis a power and cooling generation system based on geothermal flash, organic Rankine cycles, and ejector refrigeration cycle; application of zeotropic mixtures. Sustainable Energy Technol Assess 2020;40:100749.
[15] Yang J, Li Z, Yang Z, Yuanyuan D. Thermodynamic analysis and optimization of a solar organic Rankine cycle operating with stable output. Energy Convers Manage 2019;187:459–71.
[16] Roumpedakis TC, Loumpardis G, Monokrousou E, Braimakis K, Charalmapidis A, Karellas S. Exergetic and economic analysis of a solar driven small scale ORC. Renewable Energy 2020;157:1008–24.
[17] Wang M, Wang J, Zhao Y, Zhao P, Dai Y. Thermodynamic analysis and optimization of a solar-driven regenerative organic Rankine cycle (ORC) based on flat-plate solar collectors. Appl Therm Eng 2013;50:816–25.
[18] Abdollahpour A, Ghasempour R, Kasaeian A, Ahmadi MH. Exergoeconomic analysis and optimization of a transcritical CO_2 power cycle driven by solar energy based on nanofluid with liquefied natural gas as its heat sink. J Therm Anal Calorim 2020;139:451–73.
[19] Habka M, Ajib S. Performance estimation of mixtures in solar Organic Rankine Cycle with two mini cogeneration options for improvement purpose. Sustainable Energy Technol Assess 2016;16:174–89.
[20] Desai NB, Bandyopadhyay S. Thermo-economic analysis and selection of working fluid for solar organic Rankine cycle. Appl Therm Eng 2016;95:471–81.
[21] Lai NA, Wendland M, Fischer J. Working fluids for high-temperature organic Rankine cycles. Energy 2011;36:199–211.
[22] Aziz F, Salim MS, Kim MH. Performance analysis of high temperature cascade organic Rankine cycle coupled with water heating system. Energy 2019;170:954–66.
[23] Branchini L, De Pascale A, Peretto A. Systematic comparison of ORC configurations by means of comprehensive performance indexes. Appl Therm Eng 2013;61(2):471–81.
[24] Garg P, Orosz MS, Kumar P. Thermo-economic evaluation of ORCs for various working fluids. Appl Therm Eng 2016;109:841–53.
[25] Liao G, Jiaqiang E, Zhnag F, Chen J, Leng E. Advanced exergy analysis for Organic Rankine Cycle-based layout to recover waste heat of flue gas. Appl Energy 2020;266:114891.
[26] Arslan O, Kose R. Exergoeconomic optimization of integrated geothermal system in Simav, Kutahya. Energy Convers Manage 2010;51:663–76.
[27] Al-Sulaiman FA. Exergy analysis of parabolic trough solar collectors integrated with combined steam and organic Rankine cycles. Energy Convers Manage 2014;77:441–9.
[28] Acar MS, Arslan O. Energy and exergy analysis of solar energy-integrated, geothermal energy-powered Organic Rankine Cycle. J Therm Anal Calorim 2019;2019(137):659–66.
[29] Ustaoglu A, Okajima J, Zhang XR, Maruyama S. Assessment of a solar energy powered regenerative organic Rankine cycle using compound parabolic involute concentrator. Energy Convers Manage 2019;184:661–70.
[30] Askari IB, Ameri M. Solar Rankine Cycle (SRC) powered by Linear Fresnel solar field and integrated with Multi Effect Desalination (MED) system. Renewable Energy 2018;117:52–70.
[31] Xia XL, Dai GL, Shuai Y. Experimental and numerical investigation on solar concentrating characteristics of a sixteen-dish concentrator. Int J Hydrogen Energy 2012;37:18694–703.

[32] Boukelia T, Arslan O, Mecibah MS. ANN-based optimization of a parabolic trough solar thermal power plant. Appl Therm Eng 2016;107:1210–8.
[33] General Directorate of Renewable Energy of Turkish Republic. Solar atlas of Turkey, https://gepa.enerji.gov.tr/MyCalculator/; 2021 [accessed 07 March 2021].
[34] General Directorate of Renewable Energy of Turkish Republic. Solar atlas of Bilecik, https://gepa.enerji.gov.tr/MyCalculator/pages/11.aspx; 2020 [accessed 07 March 2021].
[35] General Directorate of Meteorology, Ministery of Agriculture and Forestry of Turkish Republic. Official statistics, https://www.mgm.gov.tr/veridegerlendirme/il-ve-ilceler-istatistik.aspx?m=BILECIK; 2020 [accessed 16 May 2020].
[36] Kalogirou SA. Solar energy engineering: processes and systems. 2nd ed. Elsevier Science: Academic Press; 2013.
[37] Kilic D. ANN based optimization parabolic trough type solar collector power plant: Bilecik case study. Master Thesis. Bilecik Seyh Edebali University (in Turkish); 2019.
[38] Yüksel YE. Thermodynamic assessment of modified Organic Rankine Cycle integrated with parabolic trough collector for hydrogen production. Int J Hydrogen Energy 2018;43:5832–41.
[39] EUROVENT. RS 7/C/008-2019: Rating Standard for air-cooled condensers, https://www.eurovent-certification.com/sites/default/files/2019-02/S02%20D04%20ECP-HE_2019_RS-7C008.pdf; 2020 [accessed 22 November 2020].
[40] SOLUTIA. Properties of THERMINOL-VP1, http://twt.mpei.ac.ru/tthb/hedh/htf-vp1.pdf; 2020 [accessed 16 May 2020).
[41] Mantha D, Wang T, Reddy RG. Thermodynamic modeling of eutectic point in the $LiNO_3$–$NaNO_3$–KNO_3–$NaNO_2$ quaternary system. Sol Energy Mater Sol Cells 2013;118:18–21.
[42] REFPROP. Reference Fluid thermodynamics and transport properties. NIST reference database, Version 9.0. National Institute of Standards. NIST, USA: and Technology; 2010.
[43] Bekiloglu HE, Bedir H, Anlas G. Multi-objective optimization of ORC parameters and selection of working fluid using preliminary radial inflow turbine design. Energy Convers Manage 2019;183:833–47.
[44] Kalogirou SA, Karellas S, Braimakis K, Stanciu C, Badescu V. Exergy analysis of solar thermal collectors and processes. Prog Energy Combust Sci 2016;56:106–37.
[45] Tempesti D, Manfrida G, Fiaschi D. Thermodynamic analysis of two micro CHP systems operating with geothermal and solar energy. Appl Energy 2012;97:609–17.
[46] Duffie JA, Beckman WA. Solar engineering of thermal processes. 2nd ed. New York: Wiley; 1991.
[47] Al-Sulaiman FA, Hamdullahpur F, Dincer I. Performance assessment of a novel system using parabolic trough solar collectors for combined cooling, heating, and power production. Renewable Energy 2012;48:161–72.
[48] Bassetti MC, Consoli D, Manente G, Lazzaretto A. Design and off-design models of a hybrid geothermal-solar power plant enhanced by a thermal storage. Renewable Energy 2018;128:460–72.
[49] Astolfi M, Martelli E, Pierobon L. Part 7:Thermodynamic and technoeconomic optimization of Organic Rankine Cycle systems. In: Macchi E, Astolfi M, editors. Organic rankine cycle (ORC) power systems, Woodhead Publishing; 2017, p. 173–249.
[50] Tugcu A, Arslan O, Kose R, Yamankaradeniz N. Thermodynamics and economical analysis of geothermal assisted absorption refrigeration system: Simav case study. J Turkish Soc Thermal Sci Technol 2016;36:143–59.
[51] González-Roubaud E, Pérez-Osorio D, Prieto C. Review of commercial thermal energy storage in concentrated solar power plants: steam vs. molten salts. Renew Sustain Energy Rev 2017;80:133–48.
[52] Reddy RG. Novel molten salts thermal energy storage for concentrating solar power generation. Technical Report DE-FG36-08GO18153, University of Alabama (UA), Tuscaloosa, Alabama, USA; 2013.
[53] Ministry Of Energy and Natural Resources of Turkish Republic. Electricity price for Renewables, https://www.enerji.gov.tr/tr-TR/Sayfalar/Elektrik; 2018 [accessed 30 August 2018].
[54] AlZahrani AA, Dincer I. Energy and exergy analyses of a parabolic trough solar power plant using carbon dioxide power cycle. Energy Convers Manage 2018;158:476–88.
[55] Lake A, Rezaie B. Energy and exergy efficiencies assessment for a stratified cold thermal energy storage. Appl Energy 2018;22:605–15.
[56] Alirahmi SM, Assareh E. Energy, exergy, and exergoeconomics (3E) analysis and multi-objective optimization of a multi-generation energy system for day and night time power generation - case study: Dezful city. Int J Hydrogen Energy 2020;45:61555–31573.
[57] Boukelia TE, Mecibah MS, Kumar BN, Reddy KS. Optimization, selection and feasibility study of solar parabolic trough power plants for Algerian conditions. Energy Convers Manage 2015;101:450–9.
[58] Arslan O, Acar MS. Enhanced exergetic evaluation of regenerative and recuperative coal-fired power plant. Int J Exergy 2020 (in press).
[59] Arslan O. Performance analysis of a novel heat recovery system with hydrogen production designed for the improvement of boiler effectiveness. Int J Hydrogen Energy 2021;46(10):7558–72.